AIAA SciTech Forum
11–15 & 19–21 January 2021, VIRTUAL EVENT
AIAA Scitech 2021 Forum

10.2514/6.2021-0133

Check for updates

Wind tunnel testing for hydrodynamic load characterization of icosahedron-shaped coral reef arks

Mohamed Amine Abassi[1] and Christopher Gayon[2]
San Diego State University, San Diego, CA, 92182, USA

Xiaofeng Liu[3]
San Diego State University, San Diego, CA, 92182, USA

Forest Rohwer[4]
San Diego State University, San Diego, CA, 92182, USA

Jose Castillo[5]
San Diego State University, San Diego, CA, 92182, USA

Downloaded by 72.197.174.119 on January 5, 2021 | http://arc.aiaa.org | DOI: 10.2514/6.2021-0133

Coral reefs play an important role in maintaining the balance of the marine ecosystem. They provide shelters to many marine species, protect coastlines from the damaging effects of waves and tropical storms, serve as a source of nitrogen and other essential nutrients for marine food chains and help in the process of their recycling. To promote the growth of coral reefs, an artificial structure named coral reef arks is being proposed. The arks, taking the shape of an icosahedron with a diameter of 3 meters, need to withstand ocean currents ranging from 0.5 to 2.0 m/s when deployed. To ensure the structural integrity during the arks design, wind tunnel force measurements for one solid and one hollow icosahedron models are conducted at free stream tunnel speeds of 27.2, 38.6 and 47.3 m/s, respectively, aiming to investigate the hydrodynamic characteristics of the structures. Based on the model diameter of 0.152m, the tunnel speeds give rise to corresponding Reynolds numbers of 0.26, 0.37 and 0.45 million, which correspond to ocean current speeds of 0.10, 0.14 and 0.17 m/s, respectively. The test result shows that the drag force coefficient is reduced from 0.46 to 0.37 when the test model is changing from solid to hollow icosahedron shapes. Power spectrum analysis indicates that the dominant frequencies at Strouhal numbers of 0.24 and 0.50 for the solid icosahedron model are reduced to Strouhal numbers of 0.16 and 0.19 for the hollow icosahedron model. The "ping test" clarifies that these dominant Strouhal numbers are induced by the flow rather than the natural frequencies of the structure themselves.

I. Nomenclature

f	=	Vortex shedding frequency
D	=	Model diameter
Fx	=	Side force acting on the icosahedron
Fy	=	Lift acting on the icosahedron
Fz	=	Drag acting on the icosahedron
M_x	=	Pitching moment
M_y	=	Yaw moment
M_z	=	Roll mement
Re	=	Reynolds number
V	=	Reference velocity
q	=	Dynamic pressure

[1] PhD student, Department of Aerospace Engineering, San Diego State University.
[2] Undergraduate Student, Department of Aerospace Engineering, San Diego State University.
[3] Associate Professor, Department of Aerospace Engineering, San Diego State University, Associate Fellow AIAA. Email: Xiaofeng.Liu@sdsu.edu.
[4] Professor, Department of Biology, San Diego State University.
[5] Professor, Department of Mathematics and Statistics, San Diego State University.

Copyright © 2021 by the American Institute of Aeronautics and Astronautics, Inc. All rights reserved.

υ = Kinematic viscosity
ρ = Density
T = *Temperature*
T' = *Total time duration of sampling*
S = Surface reference for the icosahedron
S_t = Strouhal number

II. Introduction

Corals are host to a wide diversity of organisms, including endosymbiotic algae, protists, fungi, bacteria, archaea, and viruses. In Professor F. Rohwer's laboratory at San Diego State University, understanding the physiological roles of these players in their interaction with the coral animal, and understanding how they relate to coral reef health is critical in maintaining the marine ecosystem balance. Incidences of coral death and disease are highly correlated with human impact[6]. To help preserve coral reefs, in addition to the biological research conducted on coral creatures, designing and building an artificial niche for marine lives contributes to the protection of the coral reef-based environment in the ocean.

Figure 1 Coral Reef Arks (https://coralarks.org/)

Artificial reefs represent one of the solutions that we can build and install in the open ocean to restore coral reefs and provide shelter for fishes, anemones, crabs, urchins, and other aquatic creatures. Different techniques and materials have been used to build such structures, e.g., using warship wrecks from World War 1 and 2 as a marine living ecosystem similar to natural coral reefs. Many technical considerations have to be taken into account to guarantee a successful artificial reef design such as stability in normal and large storms. It should be made from long lasting, solid, and non-toxic materials. Also, a good artificial reef has to have a high surface texture to be receptive to the development of corals, sponges and other organisms[7]. This paper is a part of the Coral Reef Arks collaboration effort (https://coralarks.org/) and aims to design, build and test structures that will meet the aforementioned requirements for good artificial reefs (see Figure 1). Once the ark prototype tested and approved, it will be installed in the ocean and Autonomous Reef Monitoring Structures (ARMS), as shown in Figure 2, will be affixed to it. The ARMS that will be used in the project are passive collectors used to sample marine cryptofauna[8] and will aggregate millions of reef species into one square foot structures.

Figure 2 Autonomous Reef Monitoring Structures affixed to the Coral Reef Ark (https://coralarks.org/)

The preliminary objective of our project is to propose a geometry of the coral reef ark and to test its structural stability under hydrodynamic loading. The loading response of immersed structures has been investigated for different shapes, including spherical shells (W. Ko and J. M. Stockie, 2016)[1], rectangular cantilever beams (C. A. Van Eysden and J. E. Sader, 2006)[2] and flexible hydrofoils (Abe H. Lee *et all*, 2017)[3]. To avoid any biasing regarding the flow direction around our structure, we chose a geometrical shape called regular icosahedron which is a regular polyhedron with 20 faces. This shape belongs to the family of Platonic Solids which are regular and convex polyhedra and is a member that has the highest possible number of faces in the family. Thus, it is the closest regular polyhedron to a sphere. In order to conduct experiments within our available resources at the Department of Aerospace Engineering at San Diego State University, we decided to employ our Subsonic Wind Tunnel for the low speed aerodynamic (equivalently, hydrodynamic) force and moments testing of the selected icosahedron model. Using the dynamic similarity principle, we came to the conclusion that results from the Wind Tunnel testing will be still valid for a geometrically similar system immersed in the ocean if Reynolds number is comparable. We studied two scenarios: a hollow and a solid Icosahedron. Based on power spectral analyses of the loading, we will decide which one to keep based on its frequency response and its capability to avoid resonance. A CFD analysis will also be conducted to compare with the experimentally obtained power spectral response of the aerodynamic force due to the air flow field.

[6] https://coralandphage.org/research_coral.php
[7] https://newheavenreefconservation.org/marine-blog/147-artificial-reefs-what-works-and-what-dosn-t.
[8] https://www.oceanarms.org/

Downloaded by 72.197.174.119 on January 5, 2021 | http://arc.aiaa.org | DOI: 10.2514/6.2021-0133

III. Theory

The coral reef arks that will be deployed in the ocean will undergo currents coming from different directions. To minimize the influence of the flow direction on the coral reef ark structural response, the ideal shape of the artificial reef would be as close as possible to a sphere. Because ARMS will be affixed to it, a smooth sphere will not be adequate. We need to have a regular polyhedron. The closest regular convex polyhedron (called also a Platonic Solid) to a sphere is called Icosahedron (Figure 3) that has 20 equilateral triangles faces.

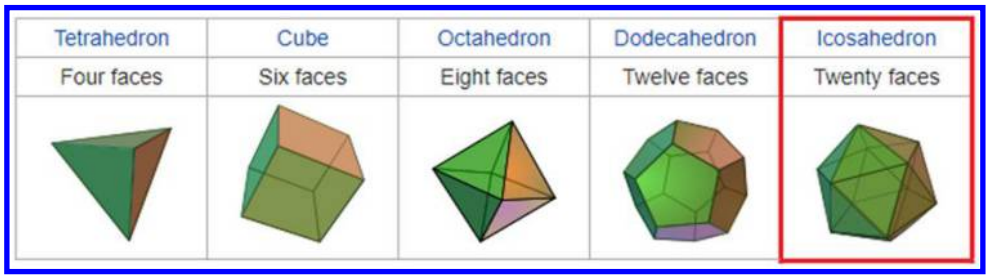

Figure 3 The family of Platonic Solids[9] (There are only 5)

After setting the shape of the coral reef ark, we have to determine the typical Reynolds number of the problem. The diameter of the structure that will be deployed in the ocean is 3 meters. The typical mean velocity of the ocean current is around 50 cm/s [10]. The average temperature in the ocean around the structure is 17°C. Therefore,

$$R_e = \frac{VL}{\nu_{water}} = \frac{0.5\times3}{1.16\times10^{-6}} = 1.2931 \times 10^6 \quad (1)$$

where $\nu_{water}(T = 17^oC) = 1.16 \times 10^{-6} m^2/s$. The maximum speed of the ocean current is around 200 cm/s, which corresponds to a Reynolds number of

$$R_e = 5.172 \times 10^6 \quad (2)$$

Instead of conducting the force measurements with water, we conducted the experiments using the Subsonic Wind Tunnel at the Department of Aerospace Engineering at San Diego State University. The air kinematic viscosity in this case is $\nu_{air} = 1.48 \times 10^{-5}$. The velocities used during the tests are as follows:

Velocities during the Wind Tunnel tests		
V_1=27.2 m/s	V_2=38.6 m/s	V_3=47.3 m/s
Re_1=260,000	Re_2=370,00	Re_3=450,000
Equivalent ocean current speeds		
V'_1=0.1 m/s	V'_2=0.14 m/s	V'_3=0.17 m/s

In the wind tunnel, in order to obtain the tunnel test speed, we use a Pitot tube to measure the dynamic pressure of the free stream flow:

$$q = \frac{1}{2}\rho_{air}V^2 \quad (3)$$

where $\rho_{air} = 1.17\ kg/m^3$. The dynamic pressure values corresponding the three velocities tested are 1.7, 3.4 and 5.1 inH_2O, respectively.

A load cell is used to measure the aerodynamic side force F_x, lift F_y, drag F_z and the pitching moment M_x, yaw moment M_y and roll moment M_z. A ping test is conducted with no flow to determine the natural frequency of the reef ark model structure. Finally, power spectral analysis will be conducted. The objective is to determine whether peak frequencies are far from the natural frequencies so as to avoid the risk of resonance and thus, ensure structural safety.

IV. Experimental Setup and Procedures

The test runs were conducted in the SDSU Subsonic Wind Tunnel. The wind tunnel is a single-return, closed jet, continuous-flow tunnel designed and constructed by the Kenny Engineering Corporation of Pasadena, California in 1963. Airflow in the wind tunnel is generated by means of a 150 HP constant speed electric motor driving a variable-pitch, 4-bladed propeller. This system provides for a continuously variable speed range in the test section from 0 to 166 mph (i.e., 0 – 74 m/s). The test section is 45" wide, 32" high and 67" long in the streamwise direction, with viewing windows on each side and on the top enabling PIV velocity diagnosis. The test section is vented at the

[9] https://en.wikipedia.org/wiki/Platonic_solid
[10] https://www.britannica.com/science/ocean-current

Downloaded by 72.197.174.119 on January 5, 2021 | http://arc.aiaa.org | DOI: 10.2514/6.2021-0133

downstream end to maintain atmospheric pressure in the test rhombus. Airflow calibration has yielded the following characteristics:

- The turbulence factor in the test section is 1.27 (i.e., turbulence intensity about 0.3%).
- The maximum deviation of dynamic pressure from the mean value does not exceed 1% at each of three survey stations; with the central survey station being located at the mid-plane of the test rhombus in the streamwise direction; the other two stations located 14" upstream and 14" downstream, respectively, from the central station.
- Flow angularity is less than ½ degree in two planes with respect to the axis of the test section within the middle half, exclusive of boundary layer.
- The static pressure variation along the longitudinal axis of the test section is less than 1.0% of mean dynamic pressure.

Two scenarios for the icosahedron shape are considered and the objective is to determine which one has better structural stability performance, as shown in Figures 4 and 5 below, respectively. The diameter of the icosahedron model D is 0.152 m. The blockage due to the model in the wind tunnel test section is 2%, indicating that the blockage is negligible.

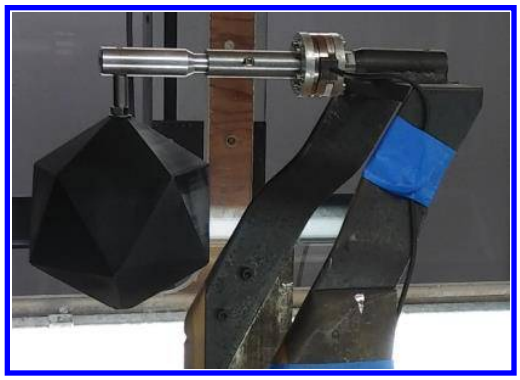

Figure 4 Solid icosahedron model in the wind tunnel

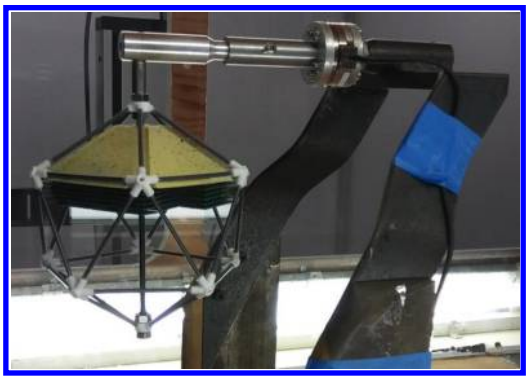

Figure 5 Hollow icosahedron model in the wind tunnel

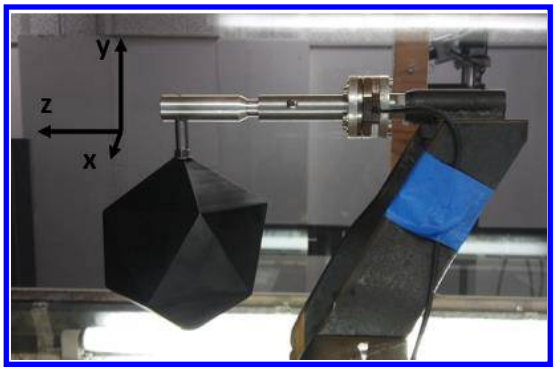

Figure 6 Reference axis orientation

Figure 7 ATI load cell (bottom), calibration box (right), extension arm (center), "part 1" (left)

As shown in Figure 6, we define the z axis to be aligned horizontally on the opposite direction of the flow. The y axis is vertical and pointing upward. The x axis is defined such that (x, y, z) is a right-handed reference.

Each model was tested in 3 different orientations/configurations (rotations about the y axis). The orientation of the model is determined by the angle between the top "leading edge" and the direction of air flow (z axis). Every 72˚ of rotation, the geometry returns to the initial position. The first orientation is when the top leading edge is aligned with the flow (z axis). The second orientation is when the top leading edge is 36˚ from the z axis. This puts the bottom leading edge of the model in the direction of the flow. Therefore, the model has been essentially flipped across the x axis. The third orientation is when the top leading edge is 18˚ from the z axis.

We use an ATI Mini 45 load cell (as shown in Figure 7) to measure the aerodynamic load on the icosahedron and the structural response during the ping test. The load cell sensor range is 120 lbf for F_x and F_y and 240 lbf for F_z. The torque range is up to 160 lbf-in. The resolution for F_x, F_y and F_z is 1/20 lbf. Similarly, the resolution of the torques M_x and M_y is 1/22 lbf and for M_z is 1/44 lbf. A Calibration box (the black box) is connected between the ATI load cell and the data acquisition box.

Downloaded by 72.197.174.119 on January 5, 2021 | http://arc.aiaa.org | DOI: 10.2514/6.2021-0133

The solid and hollow models were tested as follows: For each model (solid and hollow), three (3) different orientations were tested. For each orientation, three (3) different speeds were tested (q=1.7 inH2O, q=3.1 inH2O, q=5.4 inH2O). For each speed, 10 runs were conducted for orientation 1, and 5 runs were conducted for orientations 2 and 3 as well as the support structure only without the model on. For each run, 600,000 samples were collected over a 60 sec. sample duration with a 10kHz sample rate.

For the ping test, both the solid and hollow model were struck at 4 different locations, as shown in Figure 8.

1. The top corner of the model
2. The bottom corner of the model
3. The bottom apex of the model
4. The end of the extension arm of the stand

Five (5) runs were conducted for each of the 4 locations.

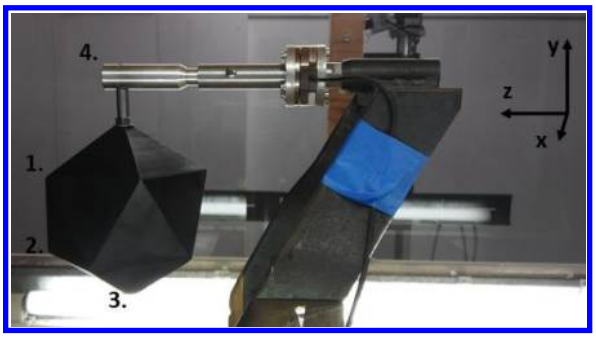

Figure 8 Locations where the model was struck during ping testing

During the analyses of the Ping test, the beginning part of the data (before the model was hit) was cut off to ensure all data files have the same length. Thus, the sample duration is not the same 60s used in the other tests.

Sample Rate	10 kHz
Sample Duration	8.19 s
Nyquist Frequency	5 kHz
Resolution	0.61 Hz
Characteristic length	0.152 m
Reference velocity	37.4 m/s

V. Results

A. Load cell data acquisition results:

The data provided by the load cell are the aerodynamic forces and the moments (with respect to x, y and z-axis respectively). We define the different aerodynamic force coefficients as follows:

$$C_i = \frac{F_{x_i}}{q.S} \;\; where\; F_{x_1} = F_x \;, F_{x_2} = F_y \;\; and\; F_{x_3} = F_z \qquad (4)$$

where q is the dynamic pressure and S is the area of the circle circumscribing the icosahedron cross section.

The moment coefficients are defined as follows:

$$C_{M_i} = \frac{M_{x_i}}{q.S.D} \;\; where\; M_{x_1} = M_x, M_{x_2} = M_y \;\; and\; M_{x_3} = M_z \qquad (5)$$

where D is model diameter. Then, the power spectral density of the aerodynamic coefficient is defined as:

$$S_{xx}(C_i) = \lim_{N\to\infty} \frac{(\Delta t)^2}{T'} \left| \sum_{n=-N}^{N} C_i(n) e^{-i2\pi f n \Delta t} \right|^2 \qquad (6)$$

where Δt is the time step, T' is the total time duration of one run and f is the frequency. The measured aerodynamic force and moment coefficients for the solid icosahedron model tested at a dynamic pressure equal to 1.7 inH_2O (V=27.2 m/s) at 3 different orientation configurations are shown in Figures 9-11.

Downloaded by 72.197.174.119 on January 5, 2021 | http://arc.aiaa.org | DOI: 10.2514/6.2021-0133

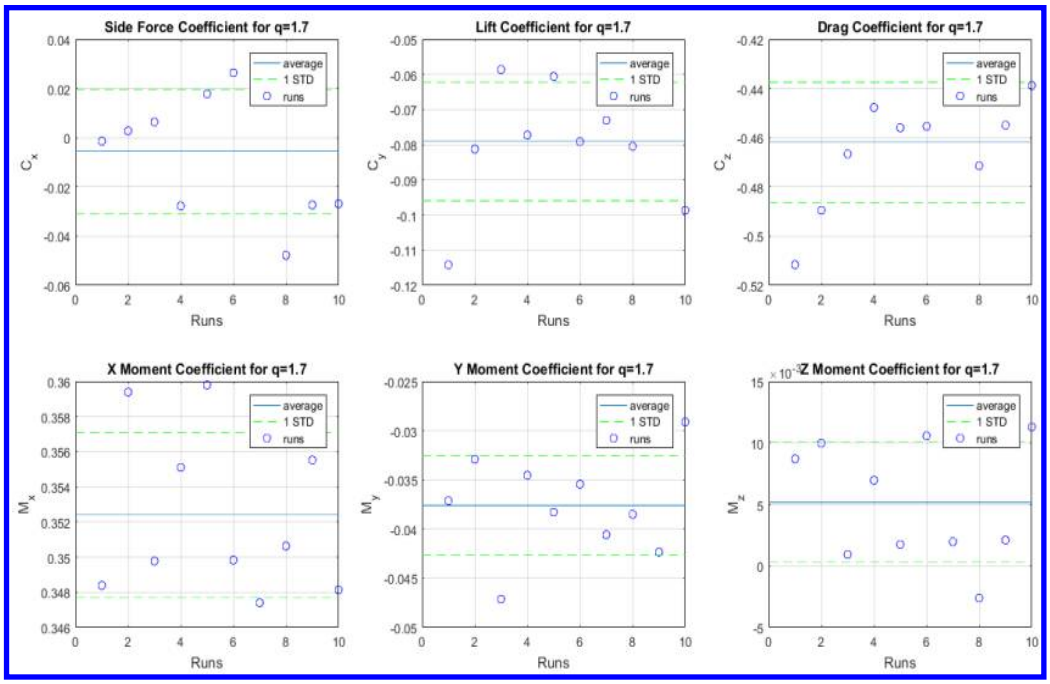

Figure 9 Force and Moment coefficients for solid icosahedron in configuration 1 tested at q=1.7 inH2O.

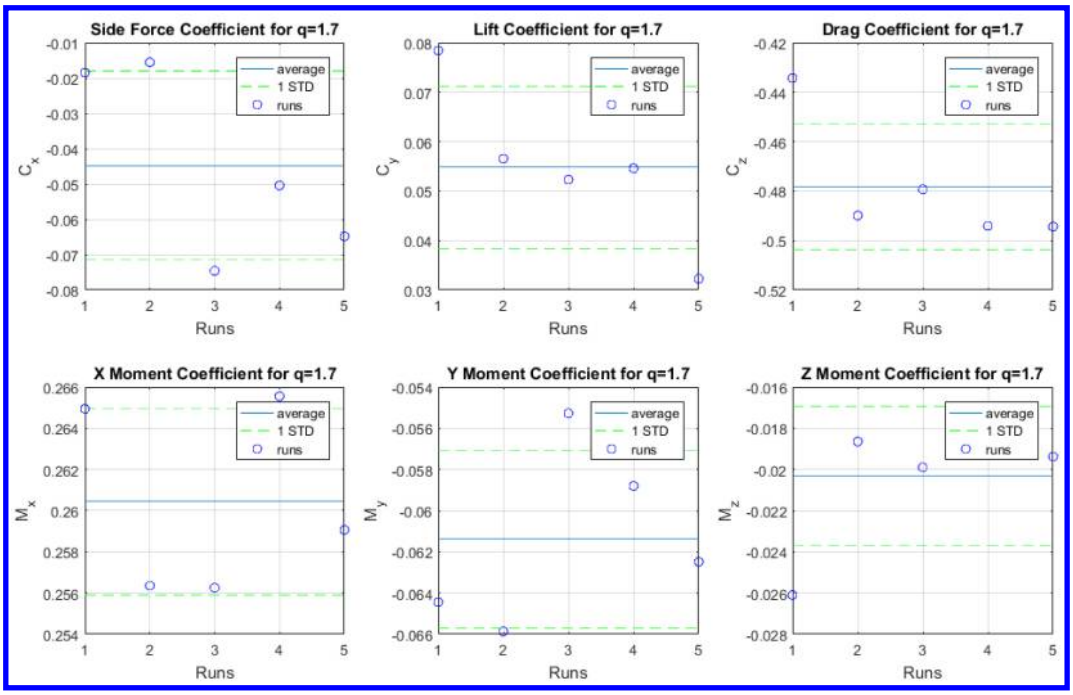

Figure 10 Force and Moment coefficients for solid icosahedron in configuration 2 tested at q=1.7 inH2O.

Downloaded by 72.197.174.119 on January 5, 2021 | http://arc.aiaa.org | DOI: 10.2514/6.2021-0133

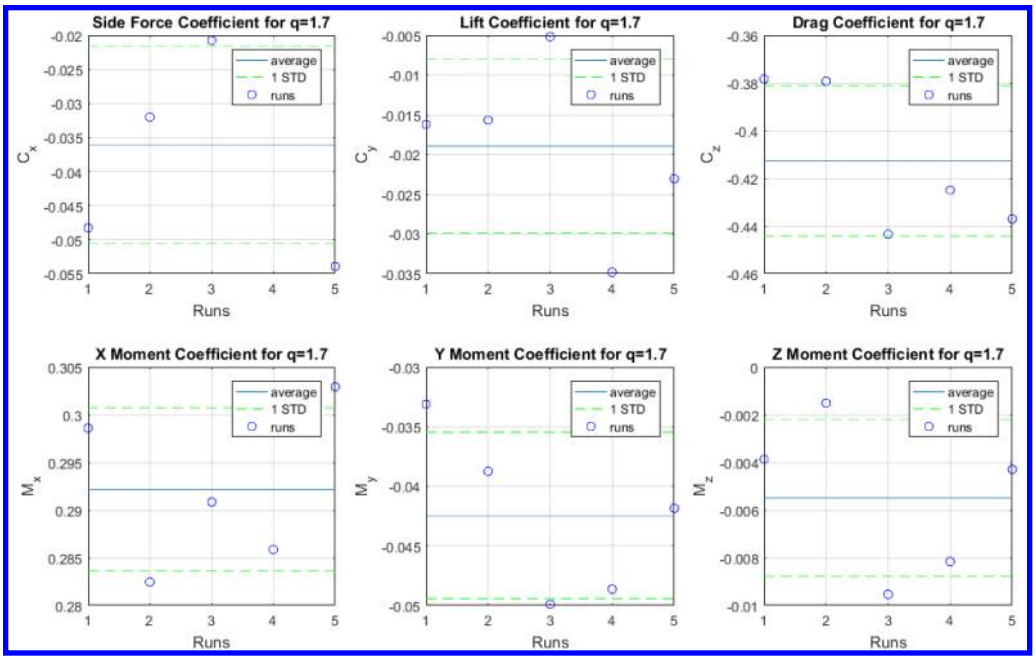

Figure 11 Force and Moment coefficients for solid icosahedron in configuration 3 tested at q=1.7 inH2O.

Figure 9 corresponding to data results in configuration 1 shows a side force coefficient average close to zero, a lift coefficient average around -0.08 and a drag coefficient equal to -0.46 with most of the runs within lines of one standard deviation. This suggests a high aerodynamic load on the z-axis and may be explained by the fact that the model at orientation configuration 1 is symmetric. The flow deviated to the left is the same to the right, and the flow deflected upward is the same downward, so they cancel out each other. Thus, we expect to have the axial loading the most important one. Figure 10 shows the results for configuration 2. Recall that this configuration has a symmetry facing the flow. The average side and lift coefficients are small (-0.045 and 0.055 respectively) compared to the drag coefficient which is -0.48.

To investigate the influence of Reynolds number on the measured aerodynamic force and moment coefficients. we calculate the different coefficients at different of Reynolds number for the three orientations, as shown in Figures 12-14, respectively.

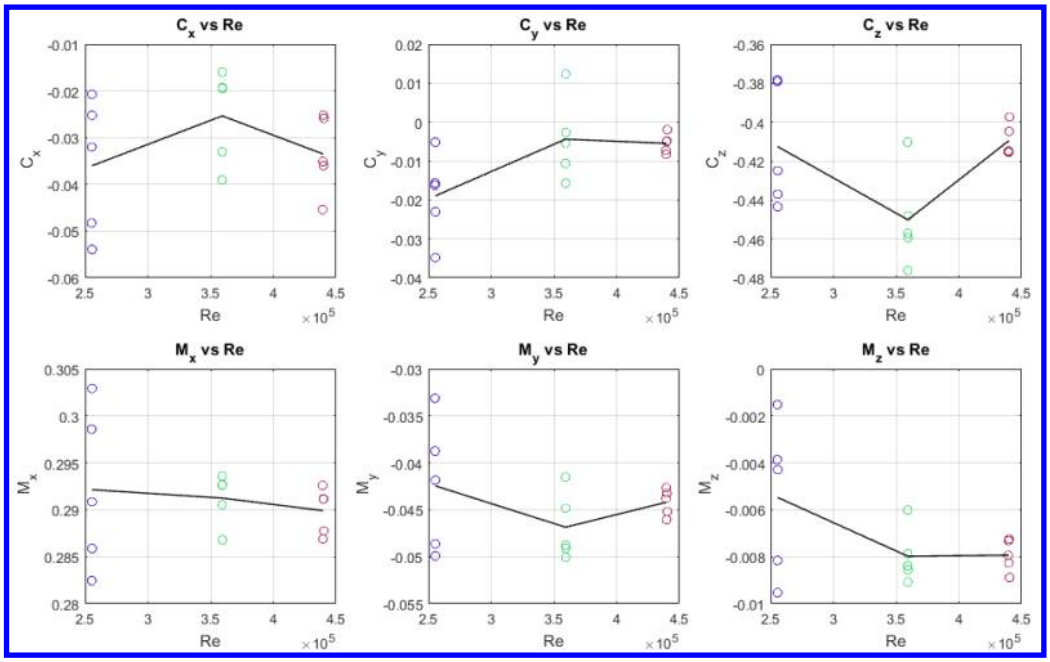

Figure 12 Force coefficients versus Reynolds number for solid icosahedron configuration 1.

Downloaded by 72.197.174.119 on January 5, 2021 | http://arc.aiaa.org | DOI: 10.2514/6.2021-0133

Downloaded by 72.197.174.119 on January 5, 2021 | http://arc.aiaa.org | DOI: 10.2514/6.2021-0133

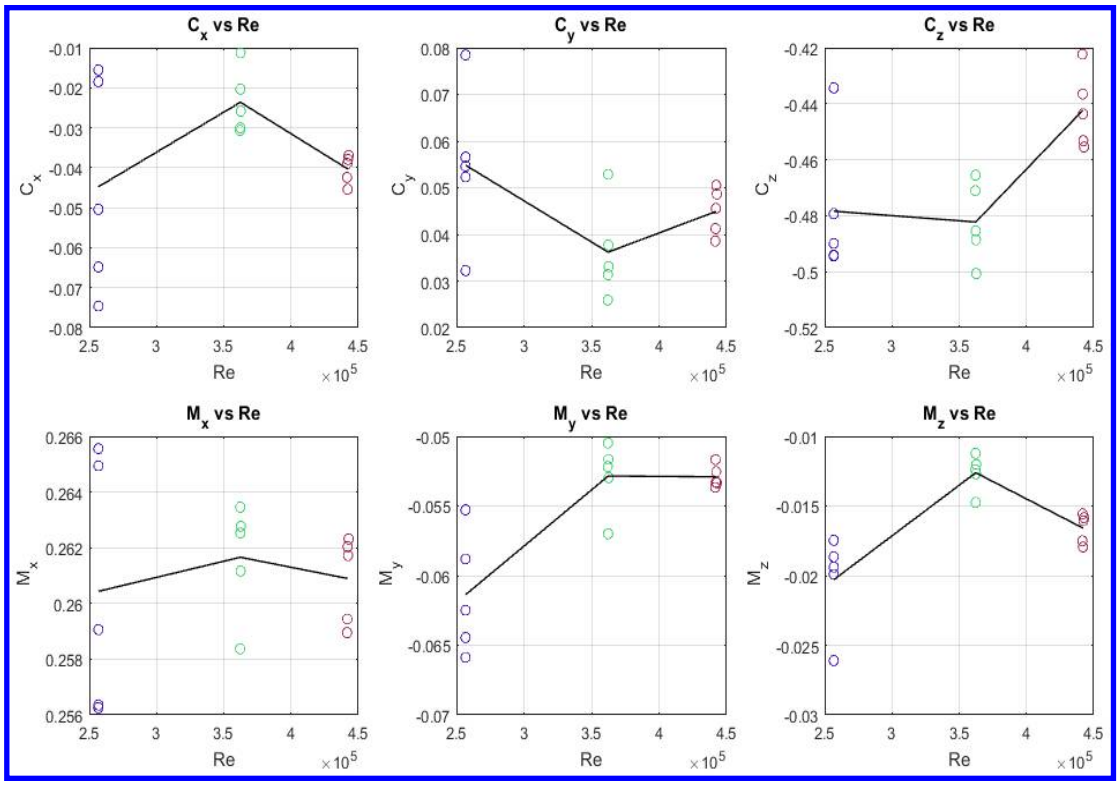

Figure 13 Force coefficients versus Reynolds number for solid icosahedron configuration 2.

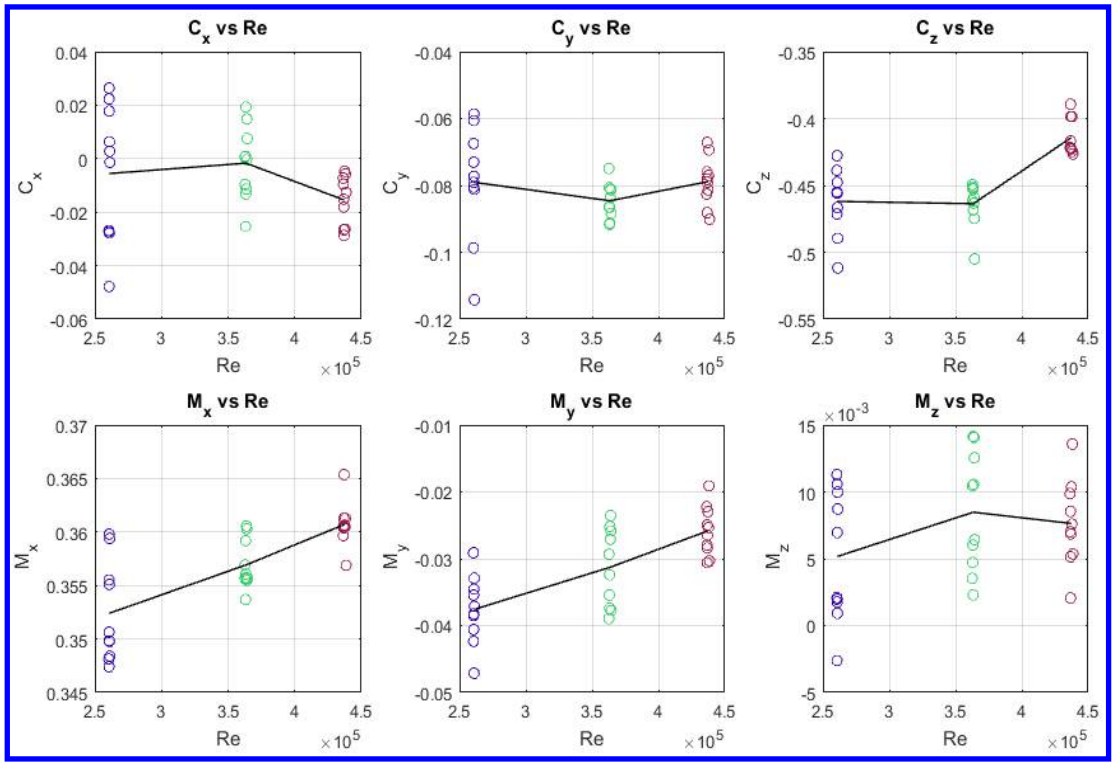

Figure 14 Force coefficients versus Reynolds number for solid icosahedron configuration 3.

As shown in Figure 12, 13 and 14, the side force coefficient fluctuates between -0.015 and -0.055. The lift coefficient fluctuates between 0.012 and -0.035. Finally, the drag coefficient fluctuates between -0.38 and -0.48. The drag coefficient is almost one order of magnitude higher than those of both lift and lateral forces.

The same analysis is conducted for the hollow icosahedron. We obtain the following data for a dynamic pressure equal to 1.7 inH_2O (V=27.2 m/s) at 3 different orientation configurations, as shown in Figures 15-17.

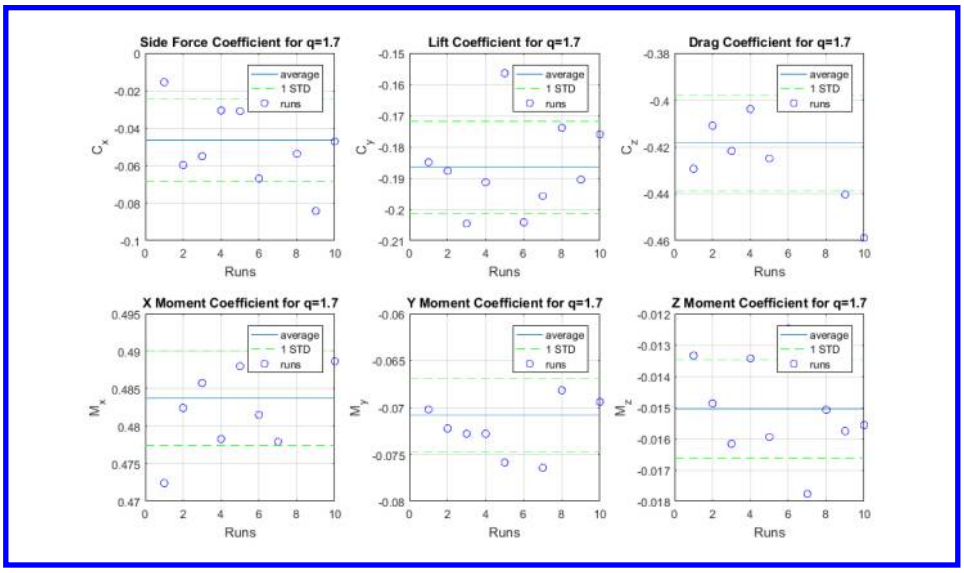

Figure 15 Force and Moment coefficients for hollow icosahedron in configuration 1 tested at q=1.7 inH2O.

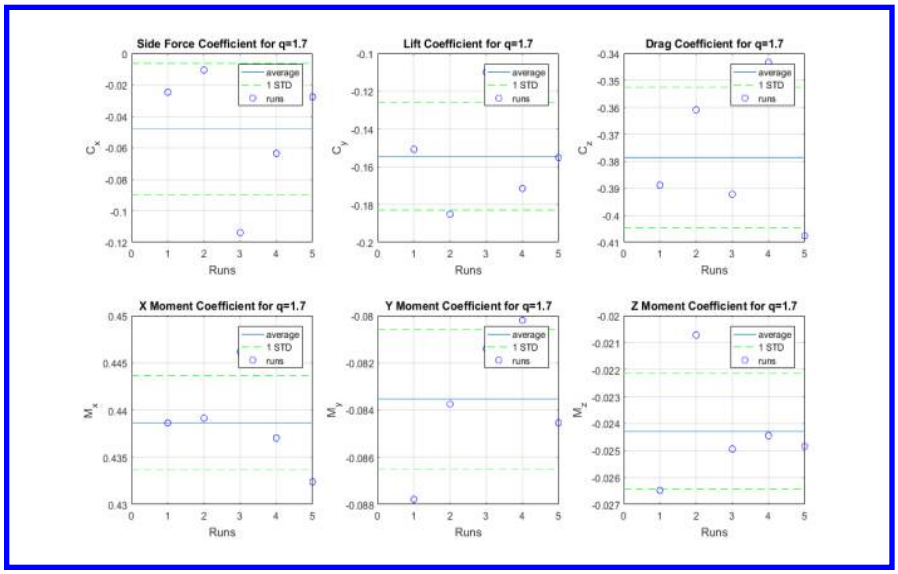

Figure 16 Force and Moment coefficients for hollow icosahedron in configuration 2 tested at q=1.7 inH2O.

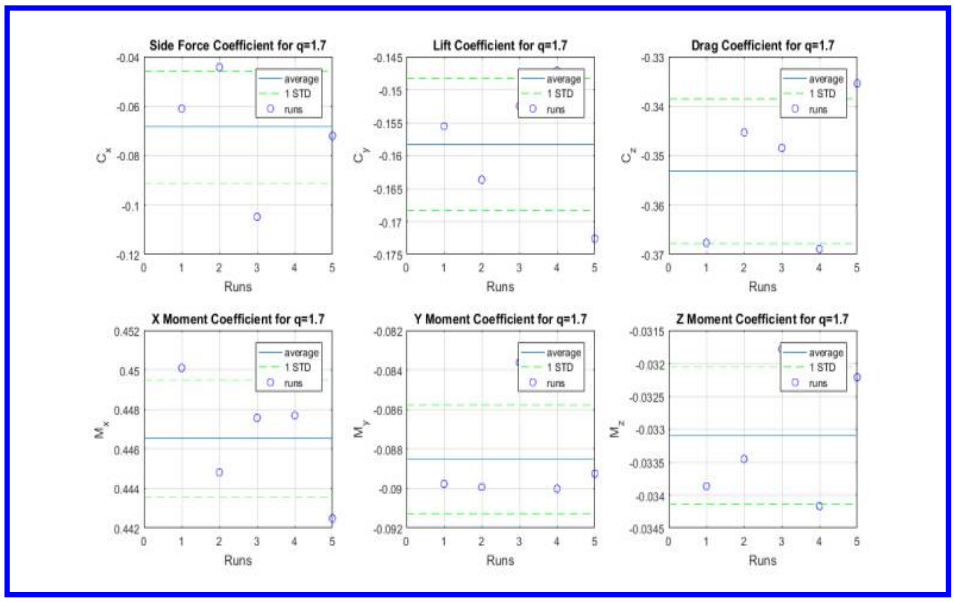

Figure 17 Force and Moment coefficients for hollow icosahedron in configuration 3 tested at q=1.7 inH2O.

Downloaded by 72.197.174.119 on January 5, 2021 | http://arc.aiaa.org | DOI: 10.2514/6.2021-0133

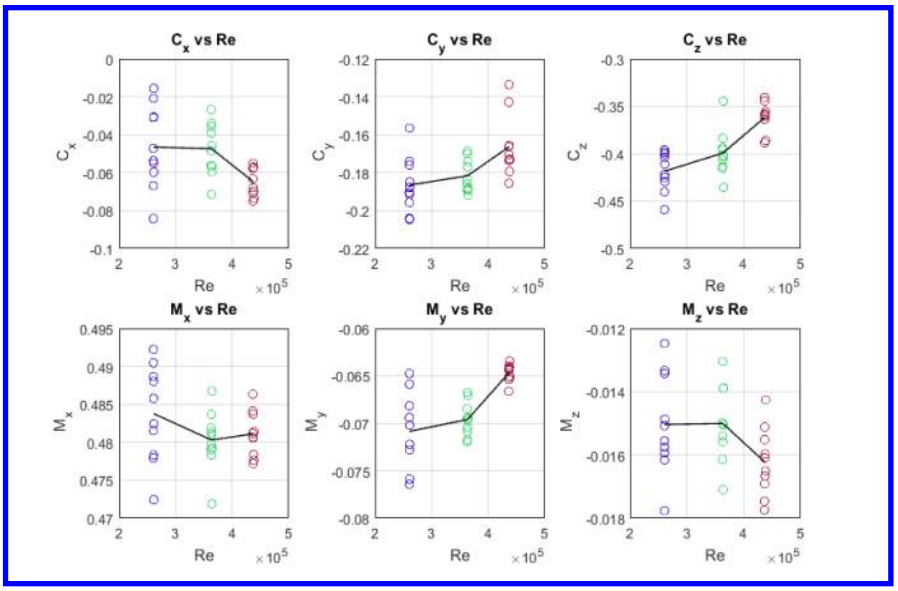

Figure 18 Force coefficients versus Reynolds number for hollow icosahedron configuration 1.

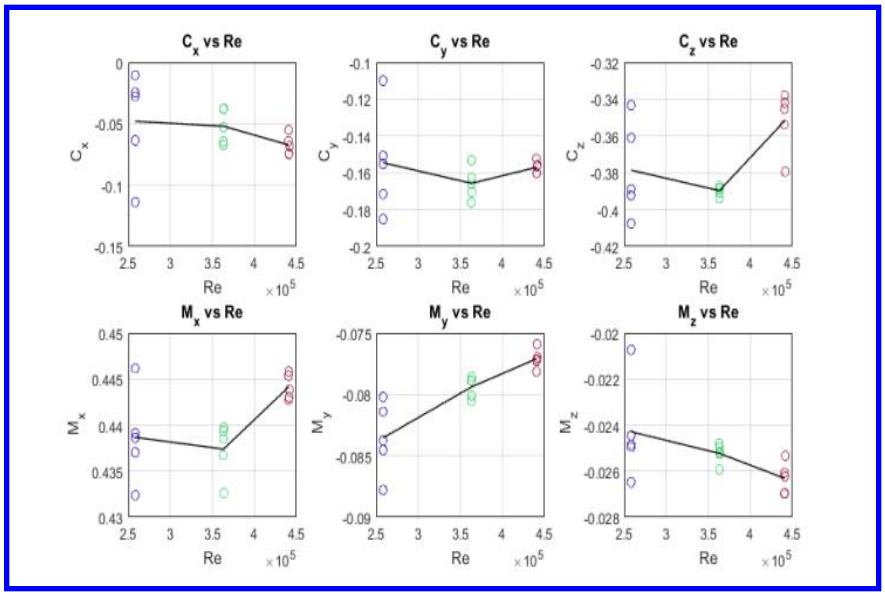

Figure 19 Force coefficients versus Reynolds number for hollow icosahedron configuration 2.

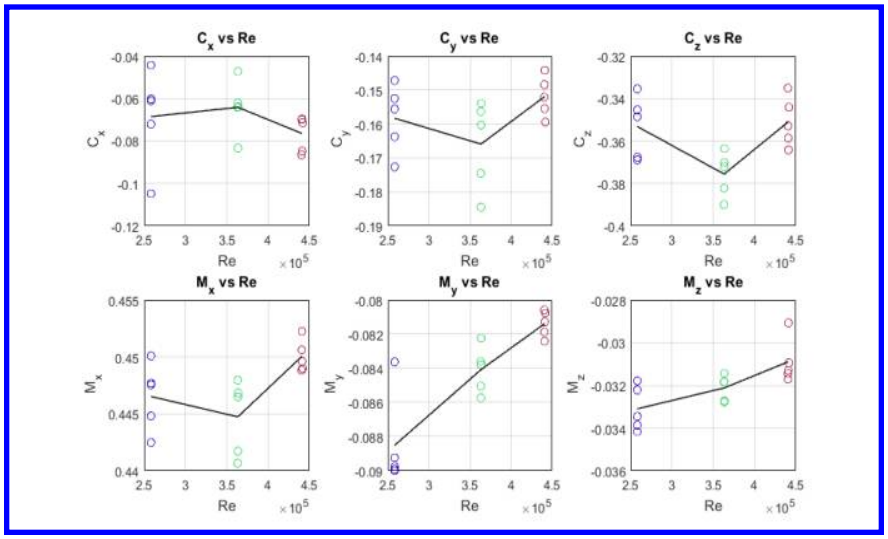

Figure 20 Force coefficients versus Reynolds number for hollow icosahedron configuration 3.

Downloaded by 72.197.174.119 on January 5, 2021 | http://arc.aiaa.org | DOI: 10.2514/6.2021-0133

Regarding the lateral force and drag coefficients, we obtain similar results to what we have obtained with the solid model. However, for the lift coefficient, we cannot say that it is negligible anymore. Figure 18, 19 and 20 confirm that this is true regardless the Reynolds number within the regime we are working in. It is important to notice that with the hollow icosahedron, we obtain smaller values for the averaged coefficients in each configuration. This may be explained by the fact that the hollow icosahedron has less frontal surface area exposed to the flow.

The following table summarizes the data for both solid and hollow models tested.

model	orientation	C_x	C_y	C_z	M_x	M_y	M_z
Hollow	1	-0.053	-0.178	-0.393	0.482	-0.068	-0.015
	2	-0.056	-0.159	-0.373	0.440	-0.080	-0.025
	3	-0.069	-0.159	-0.360	0.447	-0.085	-0.032
Solid	1	-0.008	-0.081	-0.447	0.357	-0.032	0.0071
	2	-0.036	0.045	-0.468	0.261	-0.056	-0.0165
	3	-0.032	-0.010	-0.424	0.291	-0.045	-0.0071

B. PSD analysis of the solid icosahedron:

The Power Spectral Density (PSD) analyses of the drag measurement results in comparison with that of the ping test for the solid icosahedron is shown in Figure 21. Shown in the horizontal axis in the figure is the Strouhal number $S_t = \frac{fD}{V}$, where f is frequency, D is the characteristic length and V is the reference velocity (the tunnel test speed).

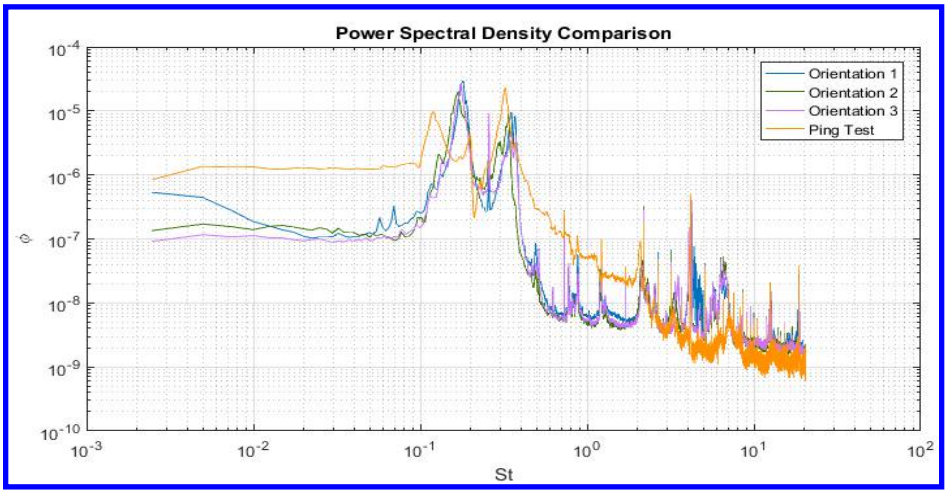

Figure 21 Ping Test and drag loading PSD for solid icosahedron.

A numerical simulation (that will be detailed later) shows a drag PSD is presented in Figure 22 below.

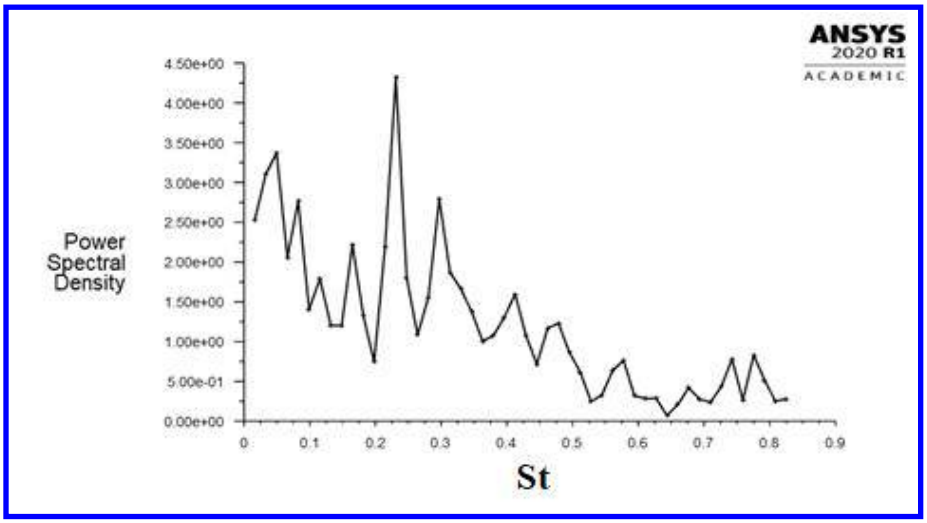

Figure 22 Drag Coefficient PSD vs St for solid icosahedron (Ansys Fluent).

Downloaded by 72.197.174.119 on January 5, 2021 | http://arc.aiaa.org | DOI: 10.2514/6.2021-0133

Figure 21 shows that the Ping test generates two important peaks at Strouhal numbers around 0.18 and 0.4. Figure 21 also shows that one of the prominent drag PSD peaks for the test model almost overlap at the same Strouhal numbers of the Ping test, suggesting that there is a risk of resonance for the solid icosahedron model. The PSD plot shown in Figure 22 indicates that the numerical simulation captures a peak drag load at Strouhal number of 0.24, very close to the Strouhal number of 0.18 which was obtained experimentally.

C. PSD analysis of the hollow icosahedron

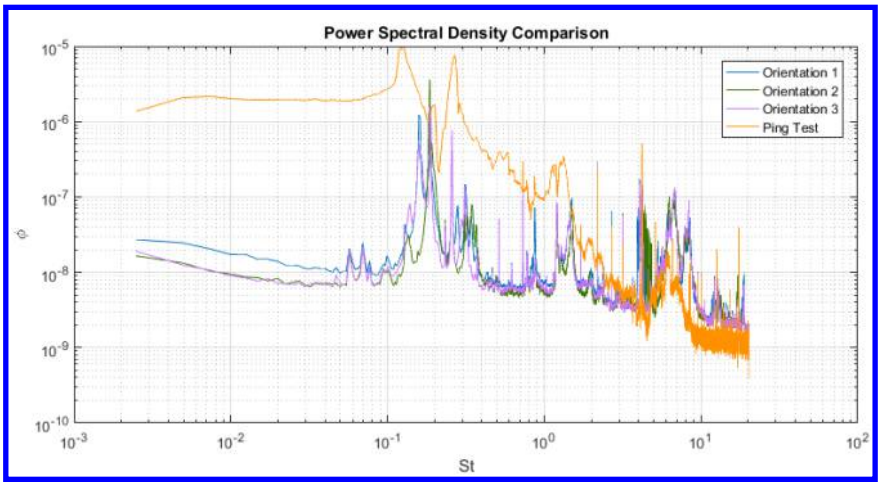

Figure 23 Ping Test Drag and loading PSD for hollow icosahedron

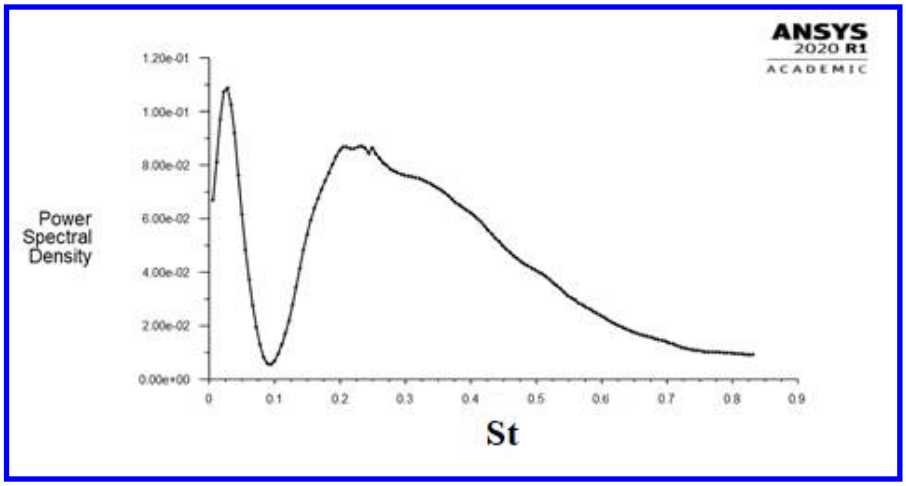

Figure 24 Drag PSD for the hollow icosahedron

Figure 23 shows that the Ping test generates two peak frequencies at Strouhal numbers slightly greater than 0.1 and at a value slightly less than 0.3. The drag PSD based on the aerodynamic test shows important peaks are between 0.2 and 0.35. However, the PSD plot based on CFD simulation (Figure 24) shows a broad frequency band from Strouhal numbers ranging between 0.15 and 0.5. This mismatch is presumably due to the limited resolution of the CFD simulation and therefore it needs to be further investigated.

D. CFD Analysis:

Using Solidworks, we designed two types of icosahedrons (Figures 25 and 26): a solid one which is opaque, and a hollow one that gives to the coral reef the opportunity to evolve and develop inside it, in addition to its permeability to water flow. Then, using Ansys Fluent, we try to describe the aerodynamic mechanism (Figures 27-30) that lays behind the different peaks in the Power Spectral diagram.

Downloaded by 72.197.174.119 on January 5, 2021 | http://arc.aiaa.org | DOI: 10.2514/6.2021-0133

Figure 25 Solidworks 3D model of the hollow Icosahedron

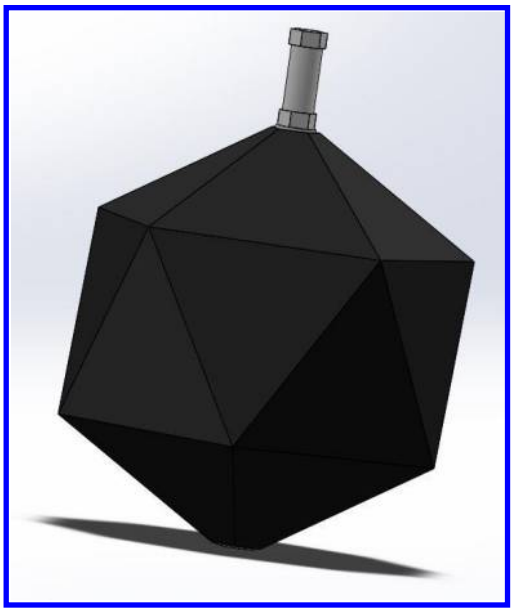

Figure 26 Solidworks 3D model of the Solid Icosahedron

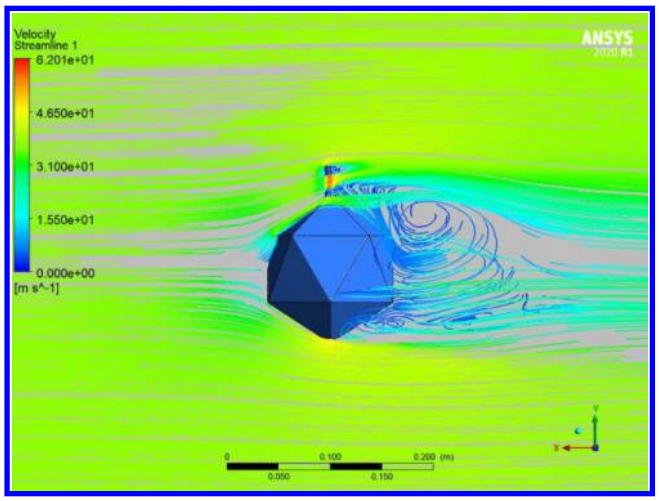

Figure 27 Streamlines around the solid model for a reference velocity=37.4 m/s at t=5 sec

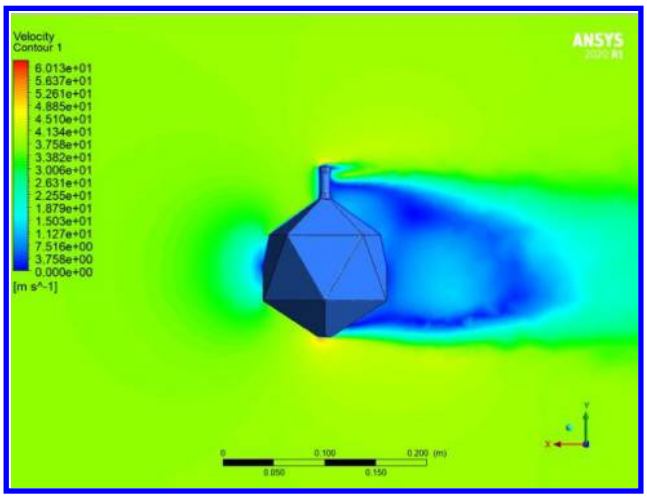

Figure 28 Contour plot of the velocity field across the solid model for a reference velocity=37.4 m/s at t=5 sec

Downloaded by 72.197.174.119 on January 5, 2021 | http://arc.aiaa.org | DOI: 10.2514/6.2021-0133

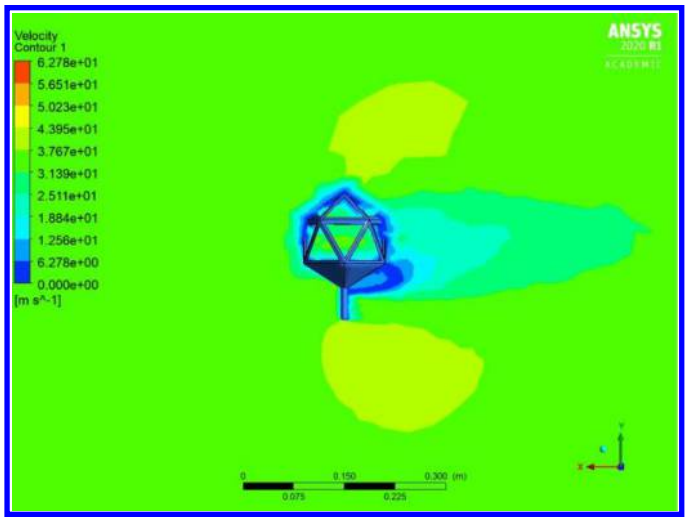

Figure 29 Contour Plot of hollow model

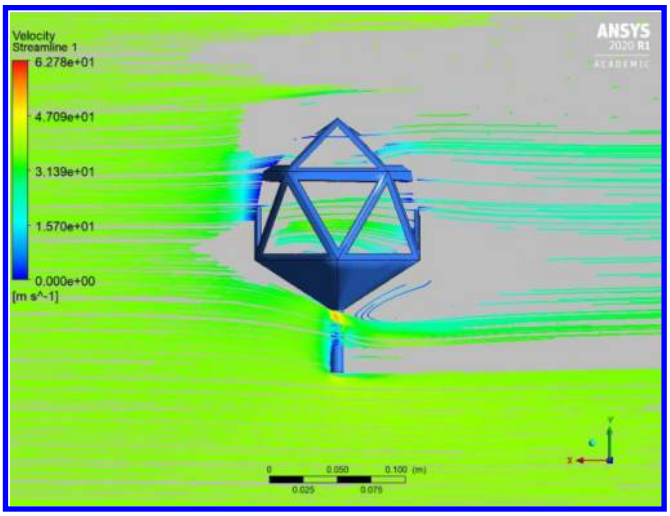

Figure 30 Streamlines in the case of hollow icosahedron

Numerical simulation graphs may give us an explanation about the reason why aerodynamic load is more important in the solid icosahedron, more than the hollow one. The wake of the solid icosahedron as seen in Figure 27 is more evident and stronger than the wake of the hollow icosahedron shown in Figure 29. This is due to the fact that we have less exposable surface in the hollow icosahedron to the air flow.

VI. Conclusion

Aerodynamic force and moment measurements of an icosahedron shaped coral reef ark model is conducted at the SDSU Subsonic Wind Tunnel to ensure the structural integrity during the arks design. One solid and one hollow icosahedron models are tested at free stream tunnel speeds of 27.2, 38.6 and 47.3 m/s, respectively. Based on the model diameter of 0.152m, the tunnel speeds give rise to corresponding Reynolds numbers of 0.26, 0.37 and 0.45 million, which correspond to ocean current speeds of 0.10, 0.14 and 0.17 m/s, respectively. The test result shows that the drag force coefficient is reduced from 0.46 to 0.37 when the test model is changing from solid to hollow icosahedron shapes. Power spectrum analysis indicates that the dominant frequencies at Strouhal numbers of 0.24 and 0.50 for the solid icosahedron model are reduced to Strouhal numbers of 0.16 and 0.19 for the hollow icosahedron model. The "ping test" clarifies that these dominant Strouhal numbers are induced by the flow rather than the natural frequencies of the structure themselves. Numerical simulation also provides useful information regarding the flow patterns over the two model configurations.

The test experiments suggest that the hollow icosahedron may be more preferable than the the solid one because of insensitivity to structural frequencies in comparison to the solid icosahedron model.

Acknowledgments

We thank Mark Hatay, technician at the SDSU Department of Physics for building the test model and Paul Ahlers, technician at SDSU Department of Aerospace Engineering for assisting the wind tunnel testing.

References

[1] W. Ko, John M. Stockie, "Parametric Resonance In Spherical Immersed Elastic Shells", *SIAM Journal of Applied Mathematics*, Vol. 76, No. 1, pp. 58-86

[2] Cornelis A. Van Eysden, John E. Sader, "Resonant frequencies of a rectangular cantilever beam immersed in a fluid" *Journal of Aircraft*, published online 10 Nov. 2016.
doi: 10.2514/1.C033040

[3] Abe H. Lee, Robert L. Campbell, Brent A. Craven, Stephen A. Hambric, "Fluid-Structure Interaction Simulation of Vortex-Induced Vibration of a Flexible Hydrofoil" *Journal of Vibration and Acoustics*, Vol. 139, 041001/ 1–12.

Downloaded by 72.197.174.119 on January 5, 2021 | http://arc.aiaa.org | DOI: 10.2514/6.2021-0133